Estimating Lagrangian transport blending drifters with HF radar data and models: Results from the TOSCA experiment in the Ligurian Current (North Western Mediterranean Sea)

Maristella Berta[a,*], Lucio Bellomo[b], Marcello G. Magaldi[a,c], Annalisa Griffa[a,d], Anne Molcard[b], Julien Marmain[b], Mireno Borghini[a], Vincent Taillandier[e]

[a]*CNR-ISMAR, La Spezia, Italy*
[b]*MIO, Université du Sud Toulon-Var, Aix-Marseille Université, CNRS/INSU, IRD, UM 110, La Garde, France*
[c]*Johns Hopkins University, Baltimore, USA*
[d]*MPO-RSMAS, University of Miami, Miami, USA*
[e]*Laboratoire d'Oceanographie de Villefranche, CNRS/UPMC, Villefranche sur Mer, France*

Abstract

Lagrangian transport estimates are investigated using results from HF radar, model and drifter data during a dedicated experiment in the Ligurian Current in the Toulon area (North Western Mediterranean Sea). Uncertainty estimates on particle position, $D(t)$, are computed and compared to absolute dispersion, $D_0(t)$, that provides an indication of the uncertainty in case of zero prior knowledge. In agreement with previous studies, radar results show that $D(t) \sim 1/2D_0(t)$ (i.e. ~ 6 km after 24 h). Model results are less reliable, as it can be expected in highly nonlinear coastal flows without local data assimilation. The central result of this paper is that when drifters are promptly deployed in an area of interest, their data can be used to significantly improve transport estimates using the Lagrangian blending algorithm LAVA with velocity fields from models or radar. Uncertainty can be reduced to $\sim 1/6D_0(t)$, (i.e. ~ 2 km after 24 h) for both radar and model, implying a much reduced search range in

*CNR-ISMAR, Forte Santa Teresa, Pozzuolo di Lerici, 19032 (SP). Italy. Tel: (+39)0187-1788916

Email address: `maristella.berta@sp.ismar.cnr.it` (Maristella Berta)

Preprint submitted to Progress in Oceanography *September 30, 2014*

case of operational applications. The method is also found to have some forecasting skills with uncertainty $\sim 1/2D_0(t)$ during the first ~ 6 hours. Sensitivity tests provide indications on relevant time and space scales of predictability and provide suggestions for appropriate drifter sampling strategies.

Keywords: LAgrangian Variational Analysis (LAVA), HF radar, drifters, Lagrangian assimilation, North Western Mediterranean Sea, Ligurian-Provençal Current.

1. Introduction

Estimates of Lagrangian transport, i.e. transport of water following quantities carried by the marine currents, play a major role in many oceanographic applications. These include search and rescue (SAR) problems, management and mitigation of oil spills and other pollutant dispersals, as well as evaluation of sediment or larval transport for coastal or fishery management. While forecasts of ocean currents are desirable for all these applications, nowcasts are also very useful especially in case of SAR or of pollutant dispersals that cannot be easily observed at all times.

Evaluating Lagrangian transport is very challenging since the motion of particles advected by ocean currents is typically chaotic, i.e. highly dependent on initial conditions and on the details of the flow [Griffa et al., 2004]. In the last decade, results from instruments such as HF coastal radars and drifters have been used in many Lagrangian transport studies of the ocean surface [Molcard et al., 2009; Shadden et al., 2009; Ullman et al., 2006]. These two types of instruments provide different and in many respects complementary information. HF radars provide maps of surface velocity with ranges up to 100 km, horizontal resolution of the order 1.5-3 km, and temporal resolution of the order of 0.25-1 h [Gurgel et al., 1999b; Harlan et al., 2010]. Drifters, on the other hand, are water following instruments, providing direct and localized information on transport [Davis, 1985]. They are influenced by motions at their own scales, of the order of 1 m in the horizontal, and communicate their position at intervals of the order of minutes for typical coastal applications. Measurements from HF radar and CODE type drifters are considered compatible in the vertical since they both sample approximately the first meter of water below the surface [Stewart and Joy, 1974]. Regarding instrument errors, drifters are subject to windage and slippage, that for CODE drifters are estimated to be within 1-3 cm/s for winds up to 10 m/s [Poulain et al., 2009]. For HF radar measurements, uncertainties are more complex and less easily quantifiable [Chapman and Graber, 1997]. They can be due to actual measurement errors related to uncalibrated antenna patterns or radio interferences [Gurgel and Barbin, 2008], but they can also be due to sea state or dependence from the methods used to reconstruct the vector velocity from the radial velocities measured by the antennas [Kohut and Glenn, 2003; Kohut et al., 2012]. Comparisons between velocity measurements from HF radars and drifters indicate typical differences of the order of 5-15 cm/s [Chapman et al., 1997; Emery et al., 2004; Essen et al., 2000; Kaplan et al., 2005; Paduan and Rosenfeld, 1996; Rypina et al., 2014; Shay et al., 1998a,b, 2001, 2007]. These differences can be due not only to the measurement errors of the two platforms, but also to the different nature of the measurements, i.e. the fact that HF radar velocities are averaged over cells of more than 1 km and over time intervals of the order of 1 h [Paduan et al., 2006; Paduan and Washburn, 2013], while drifters provide more localized spatial and temporal information. Indeed, in many cases it has been shown that the differences are within the expected environmental variability inside the radar averaging cells, such as in Mantovanelli et al. [2011], Ohlmann et al. [2007].

Another very important tool used to estimate Lagrangian transport is the use of numerical models. The accuracy of numerical models has greatly improved in the last years, in terms of resolution, data assimilation and use of specific dynamical system methods to compute transport [Haller and Poje, 1998; Olascoaga et al., 2006]. In particular, open ocean models assimilating altimetric data appear able to capture several transport features induced by large and mesoscale structures [Olascoaga and Haller, 2012]. Capturing smaller scale coastal currents and their effects on transport can be more challenging for models, unless in regions with long standing observatories [Haza et al., 2007; Kuang et al., 2012] where models have been thoroughly validated and often local in situ data are assimilated.

Lagrangian data from surface drifters or subsurface profiling floats are expected to be particularly useful for assimilation in models to improve estimates of Lagrangian transport. Various methods have been developed for Lagrangian data assimilation in the last decades [Krause and Restrepo, 2009; Kuznetsov et al., 2009; Molcard et al., 2003], and they have been tested with positive results especially for subsurface floats in open ocean [Taillandier et al., 2006b]. Assimilation of surface drifters especially in coastal regions is still challenging, since drifters provide information on the upper ocean which is highly influenced by air-sea interaction and submesoscale processes that are often only partially resolved by models. Also, the high deviation from geostrophy that is likely to dominate surface dynamics poses additional problems on the balancing of the other model state variables for assimilation. For these reasons, surface drifters have been used in a number of applications to blend rather than truly assimilate information in models [Chang et al., 2011; Taillandier et al., 2006a]. Blending corrects the surface velocity field when drifter data are available but it does not provide a complete corrected model state, so that re-initialization cannot be performed and full forecast capabilities are not provided. On the other hand, blending has the advantage that it can be quickly applied to any available velocity field and it can be very useful in many practical and operational applications for nowcast.

In particular, the LAgrangian Variational Analysis (LAVA) is a method that has been used for both, full assimilation of subsurface floats at 350 m [Taillandier et al., 2006b, 2010] and blending of surface drifters in various and different regions such as the Adriatic Sea (Mediterranean Sea) and the Kuroshio extension [Chang et al., 2011; Taillandier et al., 2008]. LAVA combines information from Lagrangian instruments with model velocity fields requiring that the distance between observed trajectories and synthetic trajectories computed from the velocity field is minimized. The method is therefore strictly Lagrangian, in the sense that it directly uses the Lagrangian position information rather than the "pseudo-Eulerian" velocity computed from the trajectories, and its correction is specifically aimed at optimizing Lagrangian transport. In principle, LAVA can be used not only to correct velocity fields from models but also from any other data source, like for example from HF radars. When other information are not available, the reconstruction of the velocity field can also be obtained with LAVA using Lagrangian data only [Taillandier et al., 2006a].

In this paper we use LAVA to blend drifter data with velocity fields from HF radars and models, as well as to reconstruct velocity from drifters only, in the French coastal area of the Ligurian Sea in front of Toulon, in the North Western Mediterranean Sea (Fig.1). While blending with model results has been tested in a number of previous applications [Chang et al., 2011; Taillandier et al., 2008], blending with HF radar is performed here for the first time, and it deserves a brief discussion to clarify its interpretation. The process of blending two data sets, each one with its peculiarity and uncertainties, is intended to provide an optimized field that takes into account the best aspects of each platform. Drifters provide local information with relatively high precision while HF radars provide extensive spatial information. The idea is to use the local information from the drifters not only to correct possible errors in the radar field (occurring for instance in case of difficult sea state, see Essen et al. [2000], or unknown antenna pattern, see Kohut and Glenn [2003]), but also and foremost to re-establish details of the environmental space variability that are smoothed by radar averaging. In case of strong horizontal shear, for instance, it can be expected that drifter information can help sharpening the velocity field increasing the gradients. This potential use of blending different data sets is investigated here, focusing on Lagrangian transport.

The goal of the work is twofold: (i) to investigate the characteristics and predictability of Lagrangian transport in a coastal area; (ii) to provide information for practical applications involving rapid response in case of accidents at sea. The work is performed in the framework of the EU-MED project TOSCA (Tracking Oil Spills and Coastal Awareness network, `http:`

//www.tosca-med.eu), that is aimed at investigating and testing science-based methodologies, best practices, and response plans in case of accidents at sea. redIn particular the TOSCA project consists in the development of a coastal monitoring and forecasting network based on HF radars and new generation drifting instruments and models, aimed at optimizing the response of local authorities to marine accidents, with a special emphasis on oil spill pollution and on SAR operations. Under this frame, the results of the present work can be useful to indicate an optimized use of HF radar and drifter data to improve estimates of Lagrangian transport.

The circulation in the study area (Fig.1(a)) was investigated with a dedicated experiment during the month of August 2012, targeting a region of the order of 50 km range, covered by a high resolution coastal model (GLAZUR64, Ourmières et al. [2011]) and by an active HF radar installation. During the experiment, a total number of 20 drifters (including redeployments) were launched, and a number of LAVA blending configurations are tested here. A first set of LAVA experiments is carried out blending the trajectories of $N_{Dft} = 7$ drifters, while the remaining 13 trajectories are used as testing for the results ("control" trajectories). To assess sensitivity to the number of drifters used in the LAVA blending, a second set of experiments is then performed downgrading N_{Dft} to 5. The LAVA algorithm is applied to both HF radar and model velocity fields, and the results of the blended fields are compared to the results of the original fields in terms of Lagrangian transport. In addition to the hindcast/nowcast capability of the system, we also test a very simplified version of "forecast", where the velocity is assumed to have a temporal persistency of the order of hours to a day. In other words, the velocity field at a given time is maintained steady over a certain period and it is used to compute Lagrangian transport. The method implies of course a simplified representation of the current field, but its testing is relevant for operational situations, to verify whether or not some guidance can be provided at least for the first few hours. It is important to keep in mind that the Mediterranean Sea has small tidal ranges being connected to the Atlantic Ocean through a narrow entrance (the Gibraltar Strait) [Arabelos et al., 2011; Pugh, 1987]. For this reason, relatively slowly varying mesoscale flows are expected to be more relevant than tidal fluctuations.

The Toulon experiment and the data from HF radars, drifters and models are described in Section 2. The description of the LAVA method is provided in Section 3 together with the description of the main diagnostics used to quantify the results. The LAVA application to HF radar and model velocities is shown in Section 4 in terms of Eulerian statistics and Lagrangian transport estimates. A summary and concluding remarks are given in Section 5.

2. The TOSCA-Toulon experiment and data sets

The TOSCA-Toulon experiment took place during the month of August 2012 in the area shown in Fig.1. The circulation in the area is part of the Ligurian/Northern Current system, that flows cyclonically along the coasts of Italy and France. The current is characterized by high variability at many scales, from seasonal to mesoscale and submesoscale. It is especially energetic during winter, with a well defined core at 10-40 km from the coast, while during summer it is weaker and often spreading offshore [Albérola et al., 1995a]. Mesoscale structures are also less energetic in summer, even though present all year round and characterized by meandering activities with periods in two main bands of approximately 3-6 and 10 days respectively [Sammari et al., 1995]. The typical Rossby radius R_d is of the order of 10 km, even though smaller structures of the order of 5 km can be found [Marullo et al., 1985]. In particular the region of Toulon is characterized by very high variability, with frequent open ocean intrusions and formation of jets and eddies [Bellomo et al., 2013; Bosse et al., 2013; Guihou et al., 2013].

During the period August 5-10, drifters were repeatedly launched from the R/V Urania. A HF radar system was operative and a high resolution model was running in real time. Drifter trajectories, model and radar coverages are all shown in Fig.1. Details on their data are given in the following.

2.1. HF radar data

The HF radar installation is based on the WERA technology [Gurgel et al., 1999a] and relies on two systems. The first one (Fort Peyras, "FP" in Fig.1) has a quasi-monostatic configuration with an irregular, W-shaped 8-antenna receiving array and 2 monopoles performing the emission while forming a zero in the direction of the receiver. The peculiarity of the receiving array geometry is imposed by the environment of the site, a dismissed military base. The second system has a bistatic configuration, with the single emitter antenna (Porquerolles island, "P" in Fig.1) located at about 17 km from the receiver (Cap Bénat, "CB" in Fig.1), a regular linear 8-antenna array.

The two systems operate at a frequency of 16.1 MHz with bandwidth of 50 kHz, giving a range resolution in the radial direction of 3 km. Antenna patterns are routinely measured almost every year. The azimuthal processing is done with the MUSIC (MUltiple SIgnal Characterization) direction finding algorithm employed routinely in CODAR [Lipa et al., 2006] and less frequently in WERA systems [Molcard et al., 2009; Sentchev et al., 2013], with a nominal 2° resolution. Current maps are produced every 20 min by integrating over the previous hour. As evidenced by Kohut et al. [2012], the vector computation accuracy partly depends on the algorithm used to compute the velocity field as well as on the Geometric Dilution Of Precision (GDOP). In this case, total velocities are computed on a regular 2 km grid with a local interpolation method which, at each cartesian grid point, minimizes the Mean Square Error (MSE) between the projection of the cartesian velocity onto the radial directions and the radial velocities available within a circle with radius 3 km [Lipa and Barrick, 1983]. To reduce errors from GDOP [Chapman et al., 1997]), totals are only computed when the angle between radial data from the two sites is within the range 30-150°, which corresponds to GDOP values smaller than 2.5.

It has been shown [Stewart and Joy, 1974] that HF radars retrieve current velocities which are vertically averaged through an exponential weighting function with a characteristic depth $\lambda_w/4\pi$, where λ_w is the wavelength of the Bragg-resonant sea waves. Since for a monostatic HF radar and approximately for a bistatic one, too, $\lambda_w = 0.5\lambda_0$, with λ_0 the electromagnetic wavelength, at the frequency at which the system was operated in our case $\lambda_w/4\pi$ gives ~75 cm for the equivalent depth.

2.2. Model data

The model configuration (GLAZUR64) is based on the primitive equation ocean circulation model NEMO [Madec, 2008]. The resolution of GLAZUR64 is uniform in the horizontal direction and set to $1/64°$ (about 1.5 km). In the vertical direction, 130 z-levels are considered with the first level at 0.5 m depth and decreasing resolution from 1 m near the surface to 30 m near the sea bed. This high-resolution three-dimensional mesh allows to well reproduce the mesoscale processes.

The model domain is shown in Fig.1 and covers the Gulf of Lions and part of the Western Ligurian Sea, featuring two open boundaries, at East and South. Initial and boundary conditions for temperature, salinity and velocity fields are provided by a large scale operational model (MERCATOR OCEAN, `http://www.mercator-ocean.fr`). MERCATOR products include assimilation of satellite data (namely, sea surface temperatures and surface level anomalies) and in situ hydrographic profiles, providing daily averaged oceanic fields on a $1/12°$ horizontal resolution with 50 vertical levels. Surface conditions rely on the atmospheric data from the Meteo-France operational regional model ARPEGE (spatial and temporal resolutions of 10 km and 3 h, respectively). Such a high spatio-temporal resolution is essential to correctly reproduce wind induced oceanic features and variability in the area, especially when the focus is on the surface circulation [Madec, 2008; Schaeffer et al., 2011].

Bulk formulation is used and requires zonal and meridional wind components at 10 m, temperature and specific humidity at 2 m, precipitation, radiative and solar fluxes. Atmospheric forcings are linearly interpolated in time. A bicubic spatial interpolation is achieved for wind forcing, while spatial linear interpolation is used for the other atmospheric forcing.

The GLAZUR64 model has been evaluated [Ourmières et al., 2011; Guihou et al., 2013] by comparing the simulations with in situ measurements and remote sensing data and it was shown to realistically simulate the Northern Current mesoscale variability at sub-regional scale.

The simulation considered here starts in June 2011 from initial conditions provided by the large scale operational model, allowing a sufficient spin-up adjustment prior to the period of interest (see Guihou et al. [2013] for a validation study of GLAZUR64).

Two-dimensional surface velocity fields used in the present analysis have a time resolution of 1 h.

2.3. Drifter data

During the Toulon experiment, 20 CODE drifters (including redeployments) were launched. CODE drifters [Davis, 1985; Poulain, 1999] measure the current in the first meter under the sea surface, and they have been chosen for the TOSCA experiment since they provide information on surface coastal circulation that is relevant for the targeted applications. Also, CODE data are expected to be compatible with HF radar data, because the equivalent integration depth is $\sim$75 cm. The drifters were equipped with Global Positioning System (GPS) receivers with an accuracy of approximately 5-10 m. Drifter positions, retrieved every 15 min, were edited to remove spikes and offsets and interpolated at uniform intervals. As observed by Edwards et al. [2006] currents measured by drifters can be partially affected by other forcings, such as wind stress and slippage. In the specific case of CODE drifters, the comparison with current meter measurements [Davis, 1985; Poulain et al., 2009] showed that drifters follow surface currents to within 3 cm/s with wind conditions up to 10 m/s. During the analyzed time windows, the wind never reached a speed comparable to this value (not shown). Moreover, Poulain et al. [2002] performed specific slippage measurements with acoustic current meters positioned at the top and at the bottom of the CODE (about 1 m apart along the vertical) and showed that drifters follow surface currents within 2 cm/s and that they are consistent with the near-surface Ekman dynamics.

During the Toulon experiment the drifters were launched in triplets and pairs characterized by an initial distance of the order of 100 m, while the typical relative distance between triplets was of the order of a few km. This deployment strategy is chosen to evidence the separation among clustered drifters due to the small scale variability and its effect on the Lagrangian transport. In fact, the experiment has a multi-scale aim: it assures a quasi-homogeneous coverage at mesoscale while providing also small scale information, as specifically investigated in Section 4.3. The overall drifter distribution is shown in Fig.1, with color-coded trajectories indicating time evolution. A first set of 14 trajectories was launched on August 5 (blue color). This set drifted mostly westward following the current and exited the radar region by August 7. Later, 6 of these drifters were picked up and redeployed in the HF radar zone on August 8 (yellow color).

3. Methodology: LAVA

LAVA is a variational method developed by Taillandier et al. [2006a] and applied in a number of cases for both full assimilation of subsurface float data and blending of surface drifters [Chang et al., 2011; Taillandier et al., 2006b, 2008]. The basic concept behind LAVA is that Lagrangian data are used to correct an available Eulerian velocity field, used as first guess, by minimizing the distance between the observed positions and the positions of numerical trajectories advected in the Eulerian field. The correction along the trajectories is spread using a diffusion equation [Derber and Rosati, 1989; Weaver and Courtier, 2001] with space scale R. The procedure is applied sequentially with individual time sequences of length T_a, given by $T_a = m\Delta t$, where m is an integer and Δt is the time step over which data are provided.

The underlying hypothesis is that T_a is significantly shorter than the persistency time of the Eulerian velocity, T_E, and also of the Lagrangian time scale of the drifter, T_L: $T_a < T_E$, $T_a < T_L$. The space scale R, on the other hand, is assumed to be of the order of the typical Rossby Radius R_d in the area, and is of course greater than the grid size Δx over which the Eulerian field is implemented.

We also notice that drifter trajectories used in LAVA are required to have a relative distance greater than $\approx 2\Delta x$, in order to avoid conflicting velocity information at the grid scale in the blending process. For this reason, given that the TOSCA experiment drifters have been launched in close triplets or pairs, the original 20 trajectories need to be subsampled for LAVA application. The maximum number of drifters obeying the requirement is $N_{Dft} = 7$, corresponding to choosing a single trajectory in each drifter group (see Fig.2). In the following, the remaining 13 trajectories are considered as control data and are used to test the LAVA results. In addition to the main configuration with $N_{Dft} = 7$, tests have also been performed downgrading the number of drifters blended in LAVA to $N_{Dft} = 5$, simply discarding some of the trajectories. In order to characterize each drifter configuration, a parameter $\overline{d_L}$ is introduced, that measures the mean initial distance between drifters used in the LAVA blending and the control ones used to test the results. The meaning and relevance of this parameter are discussed in Section 3.1.2, with reference to the introduced Lagrangian metrics.

3.1. Diagnostics of the results: Eulerian and Lagrangian metrics

The results presented in Section 4 are diagnosed using the Eulerian and Lagrangian metrics detailed below.

3.1.1. Eulerian metrics

The Eulerian metrics are designed to provide a quantitative estimate of the difference (correction C) between the original and LAVA blended velocity fields. These corrections are interpreted as an indication of the good agreement between the Eulerian velocity field and the in situ drifter data.

In Section 4, we first present a visual comparison of daily averages of the original and LAVA blended fields and of the amplitude of the vector difference between the two

$$C_{daily} = \sqrt{(< u_{or} > - < u_{LA} >)^2 + (< v_{or} > - < v_{LA} >)^2}\,, \tag{1}$$

where u and v are the two velocity components, $<>$ indicates daily averages and the subscripts u_{or}, u_{LA} indicate the original and LAVA blended velocity fields respectively.

We then provide a bulk assessment of the correction versus time, computing for each time step a spatial average value of the correction normalized by the original average value:

$$C_{norm}(t) = C_{int}(t)/U_{or}(t)\,, \tag{2}$$

where

$$\begin{aligned} C_{int} &=< \sqrt{(u_{or} - u_{LA})^2 + (v_{or} - v_{LA})^2} >_A\,, \\ U_{or} &=< \sqrt{(u_{or})^2 + (v_{or})^2} >_A\ . \end{aligned} \tag{3}$$

To preserve the contribution of all drifters, at each time t, the spatial average $<>_A$ is made over the regions where the kinetic energy of the corrected fields is at least 30% of the least energetic drifter correction. Sensitivity tests have been performed in the threshold range $10 - 50\%$ and the results are robust (not shown). The same kinetic energy criterion, applied to define the region affected by corrections, is used to perform weighted temporal averages of the velocity field reconstructed from drifters only in order to avoid biases due to the lack of velocity field estimates where drifters are not present.

3.1.2. Lagrangian metrics

Lagrangian diagnostics are designed to measure and compare the capability to estimate Lagrangian transport of original and blended velocity fields. Because Lagrangian predictability in the upper ocean is expected to be in the order of 1 day and the same time window is relevant for practical operational applications, observed trajectories are first split in segments of 24 h. Only trajectories at least 24-h long are considered and each segment is treated as a different observed trajectory in the statistics.

We first compute a simple estimate of the transport uncertainty, $D(t)$, given by the average distance at each time between the control (i.e. not used in LAVA) observed trajectories and those obtained numerically using the original and LAVA blended velocities. Specifically, numerical drifters are initialized at the same positions as the observed control drifters and are obtained integrating the Eulerian velocity in time with a fourth-order Runge Kutta scheme. Thus, $D(t)$ is defined as

$$D(t) = < \sqrt{(x_d - x_n)^2 + (y_d - y_n)^2} >_d , \tag{4}$$

where (x, y) are the components of the drifter position at time t and the subscripts d and n indicate in situ and numerical drifters, respectively. The average $<>_d$ is performed over the number of control drifters and calculated over a time period of 24 h.

At each time, $D(t)$ is compared to $D_0(t)$, i.e. the average absolute dispersion of the observed drifters over a time period of 24 h, defined as

$$D_0(t) = < \sqrt{(x_d - X_d)^2 + (y_d - Y_d)^2} >_d , \tag{5}$$

where (X_d, Y_d) are the components of the initial positions of the drifters. D_0 provides a measure of the average distance covered by drifters at each time t and is commonly referred to as "persistency error", i.e. the error that corresponds to a zero prior knowledge, i.e. assuming that particles do not move from their initial conditions [Ullman et al., 2006]. Practically, any $D(t)$ smaller than $D_0(t)$ represents an improvement with respect to a zero prior knowledge.

The metric $D(t)$ is computed averaging over control drifters that are not used in the LAVA blending and is expected to be influenced by the initial distance d_L between the control and blended drifters. We remark that since LAVA correction is spread over a range within R from the blended drifters, the LAVA assessment must be performed using control drifters within the same range R. Conceptually, we can expect that the LAVA correction is most effective near the blended trajectories, while it decreases at increasing distance from them and it vanishes at distances greater than R. As a consequence, the uncertainty estimate $D(t)$ is expected to increase at increasing values of the mean d_L. The details of this dependence might not be trivial and might be relevant for practical applications. A very small $\overline{d_L}$, of the order of $0.1 - 1$ km, corresponds to an operational situation where drifters are launched relatively close to the quantity to be monitored, for instance in case of an oil spill or SAR episode timely observed and reported. A larger $\overline{d_L}$ of a few km, on the other hand, could correspond to a case when the initial conditions of the accident are poorly known, and a large scale coverage is performed. In Section 4, we provide some insights on the dependence from $\overline{d_L}$ considering LAVA experiments with $N_{Dft} = 7$ and $N_{Dft} = 5$ drifters, that correspond to different $\overline{d_L}$. Given the overall small number of drifters (20 total) and their coverage, the number of configurations is necessarily reduced and testing is necessarily limited. Nevertheless, some indications can be drawn from the results.

3.2. LAVA experiments

In this study, 7 different LAVA experiments are configured (see Tab.1), varying the first guess Eulerian velocity fields and the parameters N_{Dft}, Δx, Δt, T_a and $\overline{d_L}$. In all the cases, R is set to 7 km, i.e. of the order of the estimated Rossby Radius R_d in the area [Marullo et al., 1985; Robinson et al., 2001].

In the first 3 experiments, E_R, E_M, E_D, the maximum number of blended trajectories is used, i.e. $N_{Dft} = 7$. The 7 drifters are shown in Fig.2, and they correspond to 5 drifters providing a good coverage of the area during a first period of ≈ 2 days, $5 - 6$ August, and other 2 situated mostly in the southern part of the domain in a second period during the last 2 days, $8 - 10$ August. A data gap occurs in the intermediate period around August 7. The corresponding parameter $\overline{d_L}$ for this drifter configuration is approximately 250 m (Tab.1), with slight value differences among the experiments because of the different discretizations of the first guess velocity, as explained below.

The parameters, Δx, Δt, T_a are chosen to retain in LAVA the highest spatial and time resolutions possible, still allowing for the optimal minimization of the misfits between positions. In the first experiment, E_R, the first guess Eulerian velocity is given by the radar, and grid size and time step are maintained as in the original fields: $\Delta x = 2$ km and $\Delta t = 20$ min. The same strategy is followed for E_M, where the first guess is given by the model fields with Δx and Δt set to 1/64° and 1 h respectively. Since radar data are more frequent in time, the analysis time scale T_a for the minimization in E_R can be chosen shorter (2 h) than for E_M (4 h).

In the third experiment, E_D, LAVA is applied with zero first guess, i.e. assuming no prior information available from models or radars, so that LAVA provides a reconstruction of the velocity based only on the positions of the drifters. For this case, LAVA parameters are set as for E_R, namely $\Delta x = 2$ km, $\Delta t = 20$ min and $T_a = 2$ h.

In the other four experiments, (E_R^{T1} E_R^{T2} E_M^{T1} E_M^{T2}, Tab.1), the sensitivity to the number of drifters used in the LAVA blending N_{Dft}, and to the configuration parameter $\overline{d_L}$ is assessed. Thus, N_{Dft} is downgraded to 5 and two $\overline{d_L}$ values are considered, namely $\overline{d_L} \approx R/4$ and $\overline{d_L} \approx R/2$. The disregarded drifters belong to the pairs/triplets around 42°39'N 6°18'E, 42°46'N 6°19'E and 42°48'N 6°17'E, respectively (Figs. 2(a) and 2(b)). In the two experiments E_R^{T1} and E_R^{T2} (E_M^{T1} and E_M^{T2}) this sensitivity is explored using the first guess Eulerian velocities from the radar (model).

In all the experiments, T_a allows to resolve the local inertial period ($T_I \sim 17$ h, Picco et al. [2010]), while original drifter positions are interpolated according to the different temporal resolutions of the velocity field in the experiments. Tab.1 summarizes all parameters for the 7 experiments.

4. Results

Results illustrate the impact of applying LAVA to the original velocity fields from radar and model. Results from the first 3 experiments, E_R, E_M, E_D, with $N_{Dft} = 7$ drifter trajectories are discussed first, in terms of Eulerian and Lagrangian metrics (Sections 4.1 and 4.2). The sensitivity of the results is then investigated via the experiments with only $N_{Dft} = 5$ drifters (Section 4.3).

Finally a discussion on the forecasting skills of the blended fields is carried out in Section 4.4.

4.1. Eulerian statistics

Examples of daily average fields are shown in Figs.2, 3 and 4 where we compare original data with those obtained from LAVA experiments E_R, E_M and E_D respectively. The evolution of the normalized correction C_{norm} (eq. 2) is shown in Fig.5.

Two examples of original radar and model daily averaged fields for days August 5 and 9 are shown in the upper panels of Fig.2 and 3 respectively. Arrows indicate velocity vectors, colors indicate velocity amplitudes, and black lines are for the drifter trajectories used in LAVA during the considered periods. In the middle panels of the same figures instead, arrows indicate LAVA blended fields while colors indicate C_{daily} (eq. 1) correction amplitudes. Finally in the lower panels, the correction vectors are shown, i.e. the differences between the LAVA blended and original velocities.

We start by discussing the radar daily averages in Fig.2. The original radar velocity (upper panels) depicts a well defined and persistent boundary current. The current is approximately zonal and flows westward along the coast (north of $\sim$42°50'N) with velocities up to 50 cm/s. The southern region is more variable and less energetic, with velocities less than 20 cm/s. Inspection of similar figures at different times t (not shown) reveals the high time variability of this area, suggestive of meanders and recirculation. A strong inertial signal (with period of $\sim$17 h) is also evident, as suggested also by drifter trajectories.

The LAVA blended fields from experiment E_R (middle panels) show very similar patterns with respect to the originals, indicating that drifter motion is in good agreement with the radar velocity. This is quantitatively shown by the C_{daily} values. During the first period (left panel), C_{daily} reaches maximum values of the order of 10 cm/s in the upper northern region where the velocities are highest, while during the second period (right panel) the corrections are significantly lower than 10 cm/s and limited to the less energetic southern region. The velocity corrections (lower panels) show a clear pattern of shear enhancement in the coastal jet during the first period.

The original model results without LAVA (Fig.3, upper panels) do not show the presence of the zonal boundary current in the northern region. Rather, the whole area is characterized by a strong meandering activity, with meridional velocities both in the inshore and offshore directions, with highest velocities of the order of 50 cm/s.

The LAVA blended fields from experiment E_M (middle panels) and the correction vectors (lower panels) present significantly different patterns from the original fields especially during the first period (left panel). In particular, the zonal boundary current can be now seen in the northern part of the domain during the first period, due to the presence of the drifters, and the correction reaches significantly higher values than for the radar, up to 30 cm/s. This is less evident in the second period (right panel), when the drifters cover only the southern region and the correction is more limited and similar to the one of the radar in magnitude. We notice that the velocity pattern depicted by the model during the first period with a high meridional shear can be indicative of meandering and jet propagations, as previously observed in this area [Guihou et al., 2013]. It is possible that the model results depict such pattern instead of a zonal current because of a time error or shift in the propagation of a perturbation, as it can happen quite commonly especially for nonlinear coastal flows in non-assimilating models.

It is interesting to compare radar and model velocities with results obtained in the experiment E_D, i.e. reconstructing the velocity fields from drifters only. The daily fields in Fig.4 show patterns highly consistent with the radar results in Fig.2, especially during the first period (left panel) when the drifter coverage extends throughout the domain. In the second period (right panel) the coverage is limited to the southern part and shows a good qualitative agreement with both radar and model fields. These results indicate that even when radar and model information are not available, the use of drifters only can lead to significant information in terms of velocity fields, of course if an adequate enough coverage is provided.

Time series of C_{norm} (eq.2) for E_R and E_M are shown in Fig.5. During the first period, with extended drifter coverage, C_{norm} is significantly higher for the model than for the radar reaching values of almost 70%, consistently with what shown by the daily results in Figs.2 and 3. The average correction (Tab.2) is almost double for the model with respect to the radar (36% and 19% respectively). During the second period, instead, when the coverage is limited to the southern region, model and radar corrections are very similar and the average is actually slightly higher for the radar (25% and 22% for E_R and E_M, respectively).

4.2. Lagrangian statistics

In order to visualize the effects of LAVA on Lagrangian transport, we first show in Fig.6 some qualitative examples of trajectories computed from original and LAVA blended radar and model velocities, comparing them with in situ drifter trajectories. The radar results (upper panels) show that the numerical trajectories computed from the original fields (green lines in left panel) are relatively similar to the drifter ones (black lines). The radar performance is further improved by the LAVA blending in the experiment E_R (purple lines in right panel). Model results (lower panels) are more striking, with trajectories from the original fields (left panel) considerably different from the drifters and in some cases diverging in opposite directions. When LAVA is applied in the experiment E_M (right panel) though, results are improved, with trajectories very close to the drifters and comparable to the radar results. This suggests that LAVA represents an effective method to enhance trajectory estimates and therefore also Lagrangian transport analysis.

A quantitative measure of the LAVA effects on transport estimates is given by the statistical quantities $D(t)$ and $D_0(t)$, (eqs.4 and 5), respectively. Results are shown in Fig.7 (left panels) for radar (upper panel) and model (lower panel). The dotted line indicates the absolute drifter dispersion $D_0(t)$ considered as a reference, reaching values of ≈12-13 km after 24 h. The radar results indicate that the trajectory uncertainty $D(t)$ computed using the original fields (pink line) grows almost linearly, reaching $\approx$6-7 km at 24 h, i.e. approximately half of $D_0(t)$. For LAVA blended E_R fields (green line), the uncertainty decreases with a maximum of 2 km at 24 h. For the model, $D(t)$ of the original field (red line) is of the same order as $D_0(t)$, actually reaching slightly higher values of 14 km at 24 h. The LAVA correction for the E_M experiment induces a striking uncertainty decrease, with maximum values less than 2 km, i.e. of the same order or smaller than the radar ones.

These results show the great advantage of using LAVA to improve transport estimates, and they suggest possible practical consequences for operational problems such as SAR or identification of pollutant spreading. In cases when no information from radar or model or other sources are available, it can be expected that a search range will be of the order of the uncertainty on particle positions quantified by the absolute dispersion $D_0(t)$, i.e. of the order of 10-15 km after 24 h in this area. When radar information are available, the results in Fig.7 suggest that the uncertainty associated with radar based trajectories $D(t)$ is approximately half than $D_0(t)$, so that the range can be decreased to approximately 6 km after 24 h. For model information, instead, at least in the case we considered, the uncertainty is of the same order of $D_0(t)$ so that the range cannot be decreased. When LAVA is applied, though, the uncertainty after 24 h is decreased to only 2 km for both radar and model, suggesting a drastic reduction in the search range.

We notice that in the case of the model, the errors corrected by LAVA are likely to be due to the nonlinear propagation of meanders that are not correctly depicted by the simulation. For the HF radar, instead, regardless the accuracy of the radar settings and the data processing algorithms, the LAVA blending is expected to improve the results because the localized drifter data restore part of the environmental variability smoothed by the radar. This is shown for instance by the enhanced shear correction in Fig.2 (lower panels).

We recall that all these results are related to hindcast or nowcast applications, while a discussion on possible forecast applications will be provided in

Section 4.4.

4.3. Sensitivity tests using downgraded configurations

All the results discussed in Sections 4.1 and 4.2 concern the first 3 experiments which blend 7 trajectories and use the remaining 13 to evaluate $D(t)$. In these experiments, $\overline{d_L}$ is approximately 250 m. Here we test the sensitivity of the $D(t)$ results considering 2 different realizations of LAVA with a reduced number of drifters, $N_{Dft} = 5$, and different values of $\overline{d_L}$, $\approx R/4$ and $\approx R/2$ respectively, while maintaining the same drifters to evaluate $D(t)$ (see Tab.1).

Results in terms of $D(t)$ are shown in Fig.7 (right panels), for radar (E_R^{T1} and E_R^{T2}, upper panel) and model (E_M^{T1} and E_M^{T2}, lower panel). The dependence on $\overline{d_L}$ can be easily seen, comparing also with the results of the main LAVA application (left panels). $D(t)$ generally increases with $\overline{d_L}$, even though at different rates between radar and model. For the radar (Fig.7b), the results of E_R^{T1} are similar to E_R with D reaching ≈2 km after 24 h, while there is a clear increase to ≈4 km for E_R^{T2}. For the model (Fig.7d), an increase to ≈3 km is already visible for E_M^{T1} while in E_M^{T2} values greater than 4 km are reached. These differences between radar and model are probably only marginally significant, given the size of standard deviations especially for the model, but it is nevertheless to be expected that the model results are more sensitive given that the LAVA correction is significantly greater than for the radar.

In summary, the results confirm that $D(t)$ increase with $\overline{d_L}$, but also suggest that the growth is relatively limited at least in the considered range, with $\overline{d_L}$ smaller than the Rossby Radius R_d. We recall in fact that R_d, in the area, is of the order of 5-10 km, comparable to the LAVA space scale R, which is set to 7 km in all experiments. Maximum values of d_L are of the order of R (not shown) and, as a consequence, the LAVA correction is still expected to be significant, and the $D(t)$ results only partially downgraded. For instance, if we compare the highest values of $D(t)$ obtained for the E_M^{T2} experiment with $D_0(t)$ and the original $D(t)$ (lower left panel), we see that the E_M^{T2} values are approximately a third of the original ones indicating a persisting significant advantage in using

LAVA. Of course if d_L values were greater than R_d, we could expect that the advantage of using LAVA will cease.

From the application point of view, the results indicate that even when the initial conditions of an accident are only approximately known or drifters are launched with a certain delay, using LAVA is still advantageous provided that drifters are launched at a relative distance between each other of order R_d. In this way, the target of interest in case of SAR or pollutant spill is expected to be at a maximum distance of the order of half R_d from the drifters used in LAVA, and the LAVA correction is expected to be significant.

4.4. Discussion on forecasting skills

All the results showed so far concern hindcast or nowcast applications. In other words, if with $[t_0, t_1]$ we indicate the time period over which model, radar and Lagrangian data are available, reconstructed LAVA trajectories and velocity fields can be provided in the interval $[t_0, t_1]$ but not for times larger than t_1. Here we test whether or not the optimized LAVA fields at time t_0 have some forecasting skills that can be used at least as a zero order approximation in operational situations. To test this question, the original and LAVA blended velocity fields at t_0 are held constant over the following 24 h and trajectories are computed using this frozen field and compared with observed drifters.

Results are shown in Fig.8 for radar (left panel) and model (right panel) in terms of $D(t)$ and $D_0(t)$. The pink (red) lines for radar (model) are obtained using the original fields while the green (blue) lines are from setups similar to E_R (E_M) experiments but with constant velocities. The radar and LAVA blended results grow with the same trend and they reach 2-4 km uncertainty on particle position during the first 6-10 h, even though LAVA results show slightly reduced $D(t)$. Nevertheless, both curves are 1 to 2 km smaller than $D_0(t)$ for the whole 24 h period, indicating that the radar and LAVA blended fields contribute to improve Lagrangian estimates. For the model, instead, LAVA leads to a significant reduction on particle position uncertainty with respect to the unblended model results. Within the very first 4 h the difference between the two curves is about 2 km and it grows up to 8 km during the whole 24 h period. This result reflects the effectiveness of the LAVA blending on the model, as previously evidenced also by the Eulerian analysis. Overall, both radar and model results show values of $D(t)$ of ≈2 km during the first 6 hours while $D_0(t)$ quickly reaches approximatively double values of 4 km. Therefore this very simple forecast approximation is advantageous during the first 6-10 h for both radar and model with respect to the zero order information represented by D_0. For the model in particular, using the LAVA blended field is especially useful and allows to improve the results with respect to the original fields.

It should be noted that these results are expected to be dependent on the correlation time scales of the Eulerian velocity field. A boundary current like the one considered here might have longer correlation times and therefore higher forecasting skills than for instance local coastal flows in gulfs or flows with large tidal fluctuations. In this case, tidal currents are extremely low (generally lower than 10^{-3}m/s) with amplitudes among the smallest in the whole Mediterranean Sea [Albérola et al., 1995b; Arabelos et al., 2011]. Even though in this paper tidal effects have been disregarded for the aforementioned reasons, we also envision possible applications of LAVA to marine basins where high frequency current variability is large. This point will be further discussed in Section 5.

5. Summary and concluding remarks

In this paper, an extensive study on estimates of Lagrangian transport based on radar, model and drifter data is presented. The study was performed during the TOSCA experiment in the Toulon region. A number of diagnostics are used, some of them of Eulerian nature, but the most relevant one is the Lagrangian diagnostic $D(t)$ that computes the distance between drifter trajectories, considered as proxy for substances advected by the currents, and numerical trajectories computed from velocity fields. The $D(t)$ diagnostic provides a quantitative measure of the uncertainty on Lagrangian transport, and it is computed for the original radar and model fields and for the LAVA blended ones. $D(t)$ is compared with the measure of drifter absolute dispersion $D_0(t)$, that quantifies how far drifters have traveled during the time t and that can be considered as the uncertainty corresponding to the case of no available information on the velocity fields.

Results show that the original radar fields reproduce well the mesoscale pattern in the area and are therefore able to provide satisfactory estimates of Lagrangian transport. $D(t)$ reaches approximately 6 km after 24 h while $D_0(t)$ is ≈12 km, indicating that the uncertainty is approximately halved using radar velocities. The situation is very different for model results, that are characterized by $D(t)$ of the same order as $D_0(t)$ indicating a non significant reduction of the uncertainty. When radar and model fields are blended with drifter data through LAVA, in both cases $D(t)$ decreases significantly, indicating that the uncertainty is strongly reduced. In quantitative terms, for LAVA experiments with 7 blended drifters, $D(t)$ is of the order of 2 km after 24 h for both radar and model. We notice that model results shown here might be a "worst case scenario", due for instance to a time lag error of the model in describing a propagating feature as it can easily occur in highly non-linear flows in absence of assimilation. The important point is that even in this difficult situation, transport estimates can be greatly improved using LAVA. For the HF radar, the improvement in the blended results is likely to be due to the fact that drifter information allow to restore part of the smoothed variability, sharpening the horizontal shear of the coastal jet. HF radar and drifters are highly correlated and they provide a better estimate of transport compared to the model without assimilating observations.

A sensitivity study is also performed considering the mean distance $\overline{d_L}$ between the drifters used in the LAVA blending and the control drifters used to compute $D(t)$, and comparing it with the analysis scale $R \approx 7$ km which is in the order of the typical Rossby radius R_d in the area. For the main configuration, $\overline{d_L}$ is ≈250 m, i.e. $\overline{d_L} \ll R$, indicating that Lagrangian transport is computed for particles initially close to the ones used for blending. Two sensitivity tests are performed with $\overline{d_L} \approx R/4$ and $R/2$, respectively. $D(t)$ increases at increasing $\overline{d_L}$ as expected, but maximum values stay below 4 km after 24 h, indicating a persistent significant advantage in using LAVA. This is especially true for the model where the uncertainty is still less than a third than for the original fields.

Finally, an investigation is carried out regarding possible forecasting skills. The velocity fields are assumed constant in time starting from a certain time t_0 and trajectories for the following period are computed using these frozen fields and compared to drifter trajectories. The results show that, especially for the model, there is a clear advantage in using LAVA blended fields, with the uncertainty that is approximately half D_0 for a period of $\approx$6 h.

Overall, results show that estimates of Lagrangian transport are significantly enhanced using LAVA blended fields. These results have a number of consequences in terms of general understanding of Lagrangian predictability in coastal flows, while also providing practical indications that can be useful for operational purposes.

From the predictability point of view, results provide quantitative information on the relevant space L and time T scales, that complement previous results obtained in other regions and from numerical models [Griffa et al., 2004; Taillandier et al., 2006a]. Regarding the space scale L, the results on $\overline{d_L}$ sensitivity indicate that the Rossby radius R_d is indeed the main parameter for Lagrangian predictability. This is not obvious a priori, since R_d is a typical Eulerian scale that characterizes the size of the most prominent features in the flow. Given the high sensitivity of Lagrangian transport to the details of the flow, it could be thought in principle that Lagrangian predictability scales L could be smaller than the Rossby radius. Our results indicate instead that R_d is indeed relevant.

Regarding the time scale T, results on the forecasting skills indicate that Lagrangian predictability is characterized by times of the order of a few hours ($\approx$6-10), typically a fraction of a day. This is much smaller than the Eulerian time scale T_E that characterizes the persistency of the features and that in our region is of the order of 3-6 days [Sammari et al., 1995]. T is likely to be related to the typical Lagrangian time scale T_L that characterizes Lagrangian velocity autocorrelation [Bauer et al., 2002]. The relationship between T_L and T_E has been studied in a number of previous papers [Lumpkin et al., 2002; Middleton, 1985; Salle et al., 2008], and is generally quite complex and dependent on the characteristics of the flow. When the flow is dominated by mesoscale structures, in the so-called "frozen-field approximation", T_L is dominated by advection processes, and typically $T_L << T_E$. When instead the flow is dominated by wind forcing or by tidal or inertial fluctuations, then $T_L \approx T_E$ and the so-called "fixed float approximation" holds. The flow field considered here is likely to be in-between the two approximations, since it is characterized by a boundary current with strong mesoscale variability [Sammari et al., 1995] but it is also subject to wind variations [Millot and Wald, 1980; Piterbarg et al., 2014] and inertial oscillations [Petrenko, 2003].

From the practical and operational point of view, the results have a number of interesting implications. In the case of SAR or pollutant detection, the improvement in transport estimates using LAVA could considerably change the range of the search. While in case of no information the range is expected to be of the order of D_0, in case of LAVA blended fields the range decreases, for instance to approximately $D_0/6$ in our experiments with 7 drifters for both radar and models. Also, if radar and model velocities are not available in the area, drifter data alone can be used to directly reconstruct the velocity field with satisfactory results, at least where the coverage is appropriate.

The results also provide suggestions on drifter sampling. When the accident location is known with accuracy, the best practice appears to be launching the drifters as close as possible to the location in space and time. When instead the accident location is not well known, as for instance for many SAR cases, then the best launching practice is to cover the region of interest with a grid size of the order of R_d. Even in this case, the LAVA blending can reduce the uncertainty to approximately $D_0/3$. Also, the method reveals some forecasting skills, so that LAVA blended fields can be used for operational purposes in a time range of approximately 6 h, still providing an uncertainty decrease of approximately $D_0/2$.

One important point is how these results can be generalized, especially regarding forecasting skills. As discussed earlier, the Lagrangian predictability scale T is expected to be related to the flow characteristics in terms of T_L and T_E. LAVA corrections and forecasting skills are expected to be more efficient in flows with a persistent mesoscale component. In cases when the flow has a large high frequency component, it might be useful to separate the two components through filtering and applying LAVA only to the mesoscale part. This is especially true when the high frequency component can be described deterministically as for instance for a tidal flow. In this case, LAVA can be used to increase mesoscale Lagrangian predictability while the high frequency part can be deterministically superimposed [Taillandier et al., 2006a] even though errors in the tidal component can occur and associated dispersion might be only partially captured.

A number of directions for future work can be envisioned. Here we have focused on the LAVA blending technique, that can be easily used in operational settings and takes advantage of any velocity field available, but that has restricted forecasting skills. Full assimilation of surface velocity data from HF radars or drifters, on the other hand, is expected to provide more extended forecasts, even though from the operational point of view it is more restricted since the model has to be appropriately set up in advance for the area. In the future, it would be useful to optimize the use of both approaches in operational settings. Also, specific technical approaches in the assimilation of surface data should be compared and further investigated. As an example, some efforts so far have concentrated on using filtered data that represent low frequency dynamics [Lipphardt et al., 2000; Oke et al., 2002], while other approaches have focused on identifying the main parameters to be optimized in a given area, such as wind forcing or boundary conditions [Barth et al., 2010, 2011; Marmain et al., 2014; Paduan and Shulman, 2004; Shulman and Paduan, 2009]. The LAVA technique could also be used to reduce radar uncertainty in emergency cases or during a rapid response operation, when radar antennas cannot be previously calibrated due to lack of time. An other important direction for further investigations is the study of optimal sampling design for drifter launchings. Here we have mostly investigated the impact on LAVA results, but it should be noted that in many practical applications other information for instance in terms of relative dispersion is desirable from closely launched clusters [Schroeder et al., 2012; Haza et al., 2013]. Optimized launchings should then combine information from various scales and different metrics. And finally, a very important issue for future studies is the improvement of drifter designs in order to make them more eco-friendly and biodegradable. This could really open new scenarios, allowing for the use of extensive drifter deployments also for operational purposes, such as a GPS-tracked version of the compact drift-card type instrument.

Acknowledgements

The authors gratefully acknowledge support from the MED TOSCA project, co-financed by the European Regional Development Fund. The GLAZUR64 simulations were performed using NEC-SX8 from GENCI-IDRIS resources (Grant 2012011707). The authors also wish to thank Mercator Ocean and Méteo-France for providing numerical data. The MIO RADAR team (Y. Barbin, J. Gaggelli, C. Quentin, P. Guterman) is also acknowledged for its major contribution to radar field campaigns of this study. M. Berta, M. G. Magaldi, A. Griffa and M. Borghini also acknowledge support form the Italian Flagship Project RITMARE. The authors also thank two anonymous reviewers for improving the manuscript.

References

Albérola, C., Millot, C., Font, J., 1995a. On the seasonal and mesoscale variabilities of the Northern Current during the PRIMO-0 experiment in the western Mediterranean Sea. Oceanologica Acta 18, 163–192.

Albérola, C., Rousseau, S., Millot, C., Astraldi, M., Font, J., Garcia-Lafuente, J., Gasparini, G.P., Send, U., Vangriesheim, A., 1995b. Tidal currents Western Mediterranean. Oceanol. Acta 18, 273–284.

Arabelos, D.N., Papazachariou, D.Z., Contadakis, M.E., Spatalas, S.D., 2011. A new tide model for the Mediterranean Sea based on altimetry and tide gauge assimilation. Oc. Sci. 7, 429–444.

Barth, A., Alvera-Azcárate, A., Beckers, J.M., Staneva, J., Stanev, E.V., Schulz-Stellenfleth, J., 2011. Correcting surface winds by assimilating High-Frequency radar surface currents in the German Bight. Ocean Dyn. 61, 599–610.

Barth, A., Alvera-Azcárate, A., Gurgel, K.W., Staneva, J., Port, A., Beckers, J.M., Stanev, E.V., 2010. Ensemble perturbation smoother for optimizing tidal boundary conditions by assimilation of High-Frequency radar surface currents-application to the German Bight. Ocean Science 6.

Bauer, S., Swenson, M.S., Griffa, A., 2002. Eddy mean flow decomposition and eddy diffusivity estimates in the tropical Pacific Ocean: 2. results. J. Geophys. Res. 107, 3154–3171.

Bellomo, L., Berta, M., Gasparini, G., Griffa, A., Magaldi, M., Marmain, J., Molcard, A., Vetrano, A., Béguery, L., Borghini, M., 2013. Observational evidence of mesoscale variability of the Northern Current (North-Western Mediterranean Sea): a combined study via gliders, HF RADAR, surface drifters, and vessel data, in: EGU General Assembly, Vienna (Austria). pp. EGU2013–5469–2.

Bosse, A., Testor, P., Mortier, L., Béguery, L., Bernardet, K., Taillandier, V., dOrtenzio, F., Prieur, L., Coppola, L., Bourrin, F., 2013. New insights of the Northern Current in the Western Mediterranean Sea from Gliders data: Mean structure, Transport, and Seasonal Variability, in: EGU General Assembly, Vienna (Austria). pp. EGU2013–11315–2.

Chang, Y., Hammond, D., Haza, A., Hogan, P., Huntley, H., Jr., A.K., Jr., B.L., Taillandier, V., Griffa, A., Ozgokmen, T., 2011. Enhanced estimation of sonobuoy trajectories by velocity reconstruction with near-surface drifters. Oc. Model. 36, 179 – 197.

Chapman, R., Graber, H., 1997. Validation of hf radar measurements. Oceanography 10, 76–79.

Chapman, R.D., Shay, L.K., Graber, H.C., Edson, J.B., Karachintsev, A., Trump, C.L., Ross, D.B., 1997. On the accuracy of HF radar surface current measurements: Intercomparisons with ship-based sensors. J. Geophys. Res. 102, 737–748.

Davis, R.E., 1985. Drifter observations of coastal surface currents during CODE: The method and descriptive view. J. Geophys. Res 90, 4741–4755.

Derber, J., Rosati, A., 1989. A global oceanic data assimilation system. J. Phys. Oceanogr. 19, 1333–1347.

Edwards, K., Werner, F., Blanton, B., 2006. Comparison of observed and modeled drifter trajectories in coastal regions: An improvement through adjustments for observed drifter slip and errors in wind fields. J. Atmos. Ocean Tech. 23, 1614–1620.

Emery, B.M., Washburn, L., Harlan, J.A., 2004. Evaluating Radial Current Measurements from CODAR High-Frequency Radars with Moored Current Meters. J. Atmos. Ocean. Technol. 21, 1259–1271.

Essen, H.H., Gurgel, K.W., Schlick, T., 2000. On the accuracy of current measurements by means of HF radar. IEEE J. Oceanic Eng. 25, 472–480.

Griffa, A., Piterbarg, L.I., Ozgokmen, T., 2004. Predictability of Lagrangian particle trajectories: Effects of smoothing of the underlying Eulerian flow. J. Marine Res. 62, 1–35.

Guihou, K., , Marmain, J., Ourmières, Y., Molcard, A., Zakardjian, B., Forget, P., 2013. A case study of the mesoscale dynamics in the North-Western Mediterranean Sea: a combined datamodel approach. Ocean Dyn. 63, 793–808.

Gurgel, K.W., Antonischki, G., Essen, H.H., Schlick, T., 1999a. Wellen Radar (WERA): a new ground-wave HF radar for ocean remote sensing. Coastal Engineering 37, 219–234.

Gurgel, K.W., Barbin, Y., 2008. Suppressing radio frequency interference in HF radars. Sea Technology 49, 39–42.

Gurgel, K.W., Essen, H.H., Kingsley, S.P., 1999b. High-Frequency radars: Physical limitations and recent developments. Coastal Engineering 37, 201–218.

Haller, G., Poje, A., 1998. Finite time transport in aperiodic flow. Physica D 119, 352–380.

Harlan, J., Terrill, E., Hazard, L., Keen, C., Barrick, D., Whelan, C., Howden, S., Kohut, J., 2010. The integrated ocean observing system high-frequency radar network: status and local, regional and national applications. Mar. Technol. Soc. J. 44, 122–132.

Haza, A., Poje, A., Ozgokmen, T., Griffa, A., Haus, B., Huntley, H., Hogan, P., Jacobs, G., Kirwan Jr., A., Lipphardt, B., Novelli, G., Olascoaga, J., Beron-Vera, F., Reniers, A., Ryan, E., 2013. Surface relative dispersion measurements in the CARTHE's grand lagrangian deployment (GLAD) experiment., in: 2013 Gulf of Mexico Oil Spill & Ecosystem Science Conference - New Orleans (USA).

Haza, A.C., Griffa, A., Martin, P., Molcard, A., Ozgokmen, T.M., Poje, A.C., Barbanti, R., Book, J.W., Poulain, P.M., Rixen, M., Zanasca, P., 2007. Model-based directed drifter launches in the Adriatic Sea: Results from the DART experiment. Geophys. Res. Lett. 34.

Kaplan, D.K., Largier, J., Botsford, L.W., 2005. HF radar observations of surface circulation off Bodega Bay (northern California, USA). J. Geophys. Res. 110, C10020.

Kohut, J., Glenn, S., 2003. Improving HF radar surface current measurements with measured antenna beam patterns. J. Atmos. Ocean Tech. 20, 1303–1316.

Kohut, J., Roarty, H., Randall-Goodwin, E., Glenn, S., Lichtenwalner, C., 2012. Evaluation of two algorithms for a network of coastal HF radars in the Mid-Atlantic Bight. Oc. Dyn. 62, 953–968.

Krause, P., Restrepo, J., 2009. The diffusion kernel filter applied to Lagrangian data assimilation. Mon. Wea. Rev. 137, 4386–4400.

Kuang, L., Blumberg, A., Georgas, N., 2012. Assessing the fidelity of surface currents from a coastal ocean model and HF radar using drifting buoys in the Middle Atlantic Bight. Ocean Dynam. 62, 1229–1243.

Kuznetsov, L., Ide, K., Jones, C., 2009. A method for assimilation of Lagrangian data. Mon. Wea. Rev. 131, 2247–2260.

Lipa, B., Nyden, B., Ullman, D.S., Terrill, E., 2006. SeaSonde Radial Velocities: Derivation and Internal Consistency. IEEE Journal of Oceanic Engineering 31, 850–861.

Lipa, B.J., Barrick, D.E., 1983. Least-Squares Methods for the Extraction of Surface Currents from CODAR Crossed-Loop Data: Application at ARSLOE. IEEE Journal of Oceanic Engineering OE-8, 226–253.

Lipphardt, B.L., Kirwan, A.D., Grosch, C.E., Lewis, J.K., Paduan, J.D., 2000. Blending HF radar and model velocities in Monterey Bay through normal mode analysis. J. Geophys. Res. 105, 3425–3450.

Lumpkin, R., Treguier, A., Speer, K., 2002. Lagrangian eddy scales in the Northern Atlantic Ocean. J. Phys. Oceanogr. 32, 24252440.

Madec, G., 2008. NEMO ocean engine, in: Technical Report, Institut Pierre-Simon Laplace, France. p. Note du Pole de modelisation.

Mantovanelli, A., Heron, M., Prytz, A., Steinberg, C., Wisdom, D., 2011. Validation of radar-based lagrangian trajectories against surface-drogued drifters in the Coral Sea, Australia, in: OCEANS 2011, pp. 1–4.

Marmain, J., Molcard, A., Forget, P., Barth, A., 2014. Assimilation of HF radar surface currents to optimize forcing in the North Western Mediterranean Sea. Nonlinear Proc. Geoph. 21, 659–675.

Marullo, S., Salusti, E., Viola, A., 1985. Observation of a small-scale baroclinic eddy in the Ligurian Sea. Deep-Sea Res. 32, 215–222.

Middleton, J.F., 1985. Drifter spectra and diffusivities. J. Marine Res. 43, 37–55.

Millot, C., Wald, L., 1980. The effect of Mistral wind on the Ligurian current near Provence. Oceanol. Acta 3, 399–402.

Molcard, A., Piterbarg, L.I., Griffa, A., Ozgokmen, T.M., Mariano, A.J., 2003. Assimilation of drifter observations for the reconstruction of the Eulerian circulation field. J. Geophys. Res. 108.

Molcard, A., Poulain, P., Forget, P., Griffa, A., Barbin, Y., Gaggelli, J., Maistre, J.D., Rixen, M., 2009. Comparison between vhf radar observations and data from drifter clusters in the gulf of la spezia (mediterranean sea). Journal of Marine Systems 78, S79–S89.

Ohlmann, C., White, P., Washburn, L., Emery, B., Terrill, E., Otero, M., 2007. Interpretation of coastal HF radarderived surface currents with high-resolution drifter data. J. Atmos. Ocean Tech. 24, 666–680.

Oke, P.R., Allen, J.S., Miller, R.N., Egbert, G.D., Kosro, P.M., 2002. Assimilation of surface velocity data into a primitive equation coastal ocean model. J. Geophys. Res. 107.

Olascoaga, M., Rypina, I., Brown, M., Beron-Vera, F., Kocak, H., Brand, L., Halliwell, G., Shay, L., 2006. Persistent transport barrier on the West Florida Shelf. Geophys. Res. Lett. 33.

Olascoaga, M.J., Haller, G., 2012. Forecasting sudden changes in environmental pollution patterns. P. Natl. Acad. Sci. USA 109, 4738–4743.

Ourmières, Y., Zakardjian, B., Béranger, K., Langlais, C., 2011. Assessment of a NEMO-based downscaling experiment for the North-Western Mediterranean region: Impacts on the Northern Current and comparison with ADCP data and altimetry products. Ocean Mod. 39, 386–404.

Paduan, J., Kim, K.C., Cook, M., Chavez, F., 2006. Calibration and validation of direction-finding high-frequency radar ocean surface current observations. IEEE J. Oceanic Eng. 31, 862–875.

Paduan, J.D., Rosenfeld, L.K., 1996. Remotely sensed surface currents in Monterey Bay from shore based HF radar (Coastal Ocean Dynamics Application Radar). J. Geophys. Res. 101, 20669–20686.

Paduan, J.D., Shulman, I., 2004. HF radar data assimilation in the Monterey Bay area. J. Geophys. Res 109.

Paduan, J.D., Washburn, L., 2013. High-frequency radar observations of ocean surface currents. Annu. Rev. Mar. Sci. 5, 115–136.

Petrenko, A.A., 2003. Variability of circulation features in the Gulf of Lion NW Mediterranean Sea. Importance of inertial currents. Oceanol. Acta 26, 323–338.

Picco, P., Cappelletti, A., Sparnocchia, S., Schiano, M., Pensieri, S., Bozzano, R., 2010. Upper layer current variability in the Central Ligurian Sea. Ocean Sci. 6, 825–836.

Piterbarg, L., Taillandier, V., Griffa, A., 2014. Investigating frontal variability from repeated glider transects in the Ligurian Current (North West Mediterranean Sea). J. Marine Syst. 129, 381–395.

Poulain, P.M., 1999. Drifter observations of surface circulation in the Adriatic Sea between December 1994 and March 1996. J. Marine Syst. 20, 231 – 253.

Poulain, P.M., Gerin, R., Mauri, E., Pennel, R., 2009. Wind effects on drogued and undrogued drifters in the Eastern Mediterranean. J. Atmos. Ocean Tech. 26, 1144–1156.

Poulain, P.M., Ursella, L., Brunetti, F., 2002. Direct measurements of water-following characteristics of CODE surface drifters, in: LAPCOD Meeting.

Pugh, D.T., 1987. Tides, Surges and Mean Sea-Level. John Wiley and Sons, New York.

Robinson, A., Leslie, W., Theocharis, A., Lascaratos, A., 2001. Mediterranean Sea circulation, in: Steele, J.H., Thorpe, S.A., Turekian, K.K. (Eds.), Ocean currents: a derivative of the encyclopedia of ocean sciences. Academic press San Diego.

Rypina, I.I., Kirincich, A.R., Limeburner, R., Udovydchenkov, I.A., 2014. Eulerian and Lagrangian Correspondence of High-Frequency Radar and Surface Drifter Data: Effects of Radar Resolution and Flow Components. J. Atmos. Ocean. Technol. 31, 945–966.

Salle, J.B., Speer, K., Morrow, R., Lumpkin, R., 2008. An estimate of Lagrangian eddy statistics and diffusion in the mixed layer of the Southern Ocean. J. Marine Res. 66, 441–463.

Sammari, C., Millot, C., Prieur, L., 1995. Aspects of the seasonal and mesoscale variabilities of the Northern Current in the western Mediterranean Sea inferred from the PROLIG-2 and PROS-6 experiments. Deep-Sea Res. 42, 893–917.

Schaeffer, A., Molcard, A., Forget, P., Fraunie, P., Garreau, P., 2011. Generation mechanisms for mesoscale eddies in the Gulf of Lions: radar observation and modeling, in: Ocean Dyn., pp. 1587–1609.

Schroeder, K., Chiggiato, J., Haza, A.C., Griffa, A., Ozgokmen, T.M., Zanasca, P., Molcard, A., Borghini, M., Poulain, P.M., Gerin, R., Zambianchi, E., Falco, P., Trees, C., 2012. Targeted Lagrangian sampling of submesoscale dispersion at a coastal frontal zone. Geophys. Res. Lett. 39.

Sentchev, A., Forget, P., Barbin, Y., Yaremchuk, M., 2013. Surface circulation in the Iroise Sea (W. Brittany) from high resolution HF radar mapping. Journal of Marine Systems 109-110, S153–S168.

Shadden, S.C., Lekien, F., Paduan, J.D., Chavez, F.P., Marsden, J.E., 2009. The correlation between surface drifters and coherent structures based on high-frequency radar data in Monterey Bay. Deep-Sea Res. Pt II 56, 161 – 172.

Shay, L.K., Cook, T.M., Hallock, Z., Haus, B.K., Graber, H.C., Martinez, J., 2001. The Strength of the m_2 Tide at the Chesapeake Bay Mouth. J. Phys. Oceanogr. 31, 427–449.

Shay, L.K., Lee, T.N., Williams, E.J., Graber, H., Rooth, C.G.H., 1998a. Effects of low-frequency current variability on submesoscale near-inertial vortices. J. Geophys. Res. 103, 18691–18714.

Shay, L.K., Lentz, S.J., Graber, H.C., Haus, B.K., 1998b. Current Structure Variations Detected by High-Frequency Radar and Vector-Measuring Current Meters. J. Atmos. Ocean. Technol. 15, 237–256.

Shay, L.K., Martinez-Pedraja, J., Cook, T.M., Haus, B.K., Weisberg, R.H., 2007. High Frequency Radar Mapping of Surface Currents Using WERA. J. Atmos. Ocean. Technol. 24, 485–503.

Shulman, I., Paduan, J.D., 2009. Assimilation of HF radar-derived radials and total currents in the Monterey Bay area. Deep Sea Res. Pt. II 56, 149 – 160.

Stewart, R.H., Joy, J.W., 1974. HF radio measurements of surface currents. Deep-Sea Res. 21, 1039–1049.

Taillandier, V., Dobricic, S., Testor, P., Pinardi, N., Griffa, A., Mortier, L., Gasparini, G.P., 2010. Integration of Argo trajectories in the Mediterranean Forecasting System and impact on the regional analysis of the western Mediterranean circulation. J. Geophys. Res. 115.

Taillandier, V., Griffa, A., Molcard, A., 2006a. A variational approach for the reconstruction of regional scale Eulerian velocity fields from Lagrangian data. Oc. Model. 13.

Taillandier, V., Griffa, A., Poulain, P.M., Branger, K., 2006b. Assimilation of Argo float positions in the north western Mediterranean Sea and impact on ocean circulation simulations. Geophys. Res. Lett. 33.

Taillandier, V., Griffa, A., Poulain, P.M., Signell, R., Chiggiato, J., Carniel, S., 2008. Variational analysis of drifter positions and model outputs for the reconstruction of surface currents in the central Adriatic during fall 2002. J. Geophys. Res. 113.

Ullman, D.S., O'Donnell, J., Kohut, J., Fake, T., Allen, A., 2006. Trajectory prediction using HF radar surface currents: Monte Carlo simulations of prediction uncertainties. J. Geophys. Res. 111.

Weaver, A., Courtier, P., 2001. Correlation modelling on the sphere using a generalized diffusion equation. Quart. J. Roy. Meteor. Soc. 127, 1815–1846.

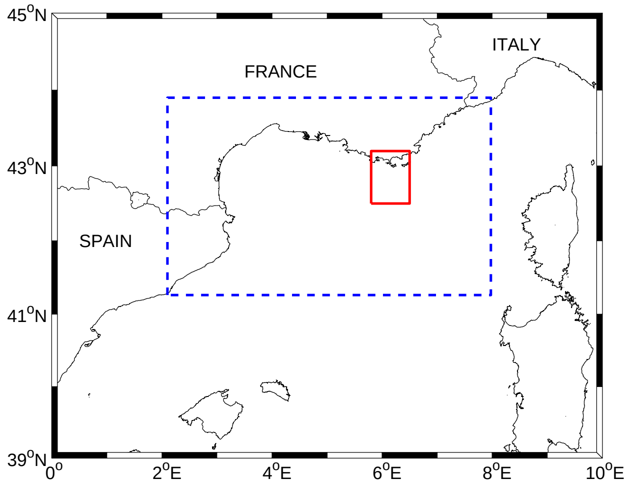

(a)

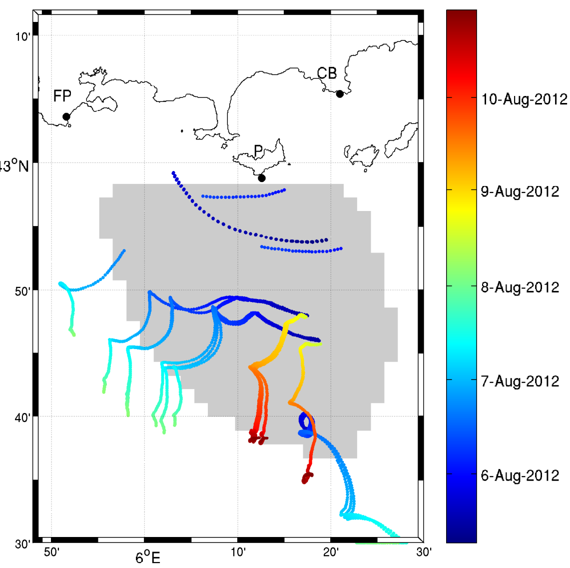

(b)

Figure 1: (a) Western Mediterranean basin. The dashed blue line represents the limits of the GLAZUR64 model domain. The red solid square indicates the area of the experiment in front of Toulon (France), expanded in panel (b) where the gray area is the radar coverage, the black dots show the radar sites (FP-Fort Peyras, P-Porquerolles and CB-Cap Bénat). The whole set of 20 drifter trajectories are color coded for time during the period from 5-Aug-2012 06:41:00 to 10-Aug-2012 22:21:00 (UTC times). The domain width is chosen to give an overview on drifters and close trajectories may not be distinguishable.

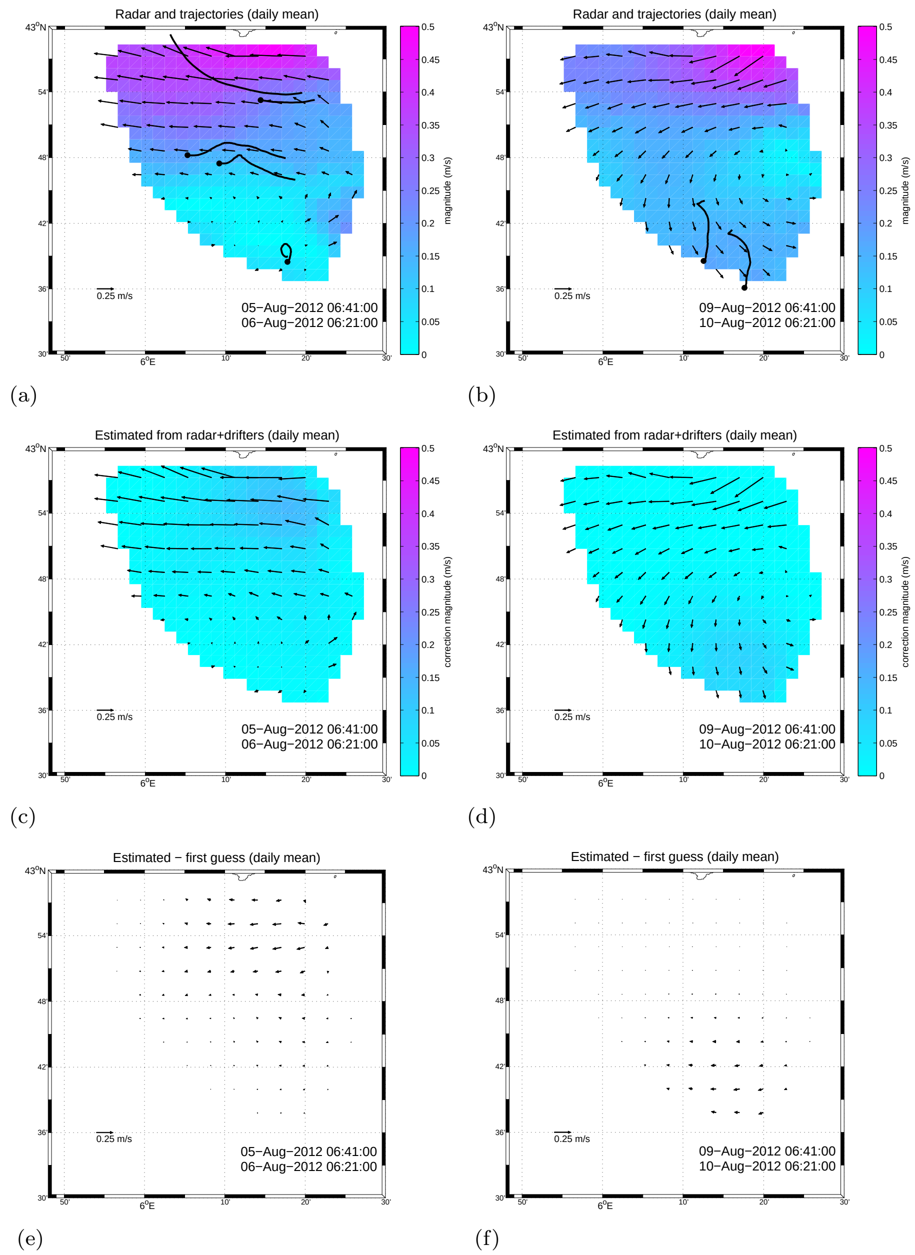

Figure 2: Examples of daily average radar velocities for August 5 (left panels) and August 9 (right panels). (a) and (b) show the original velocity fields, with color indicating velocity amplitude and arrows indicating velocity vectors. Drifter trajectories used in LAVA are superimposed; (c),(d) show the LAVA blended fields (E_R), with color indicating the amplitude of the correction C_{daily} (equation 1) and arrows indicating velocity vectors. Panels (e) and (f) represent the vectorial difference between the LAVA estimated and the original velocity field.

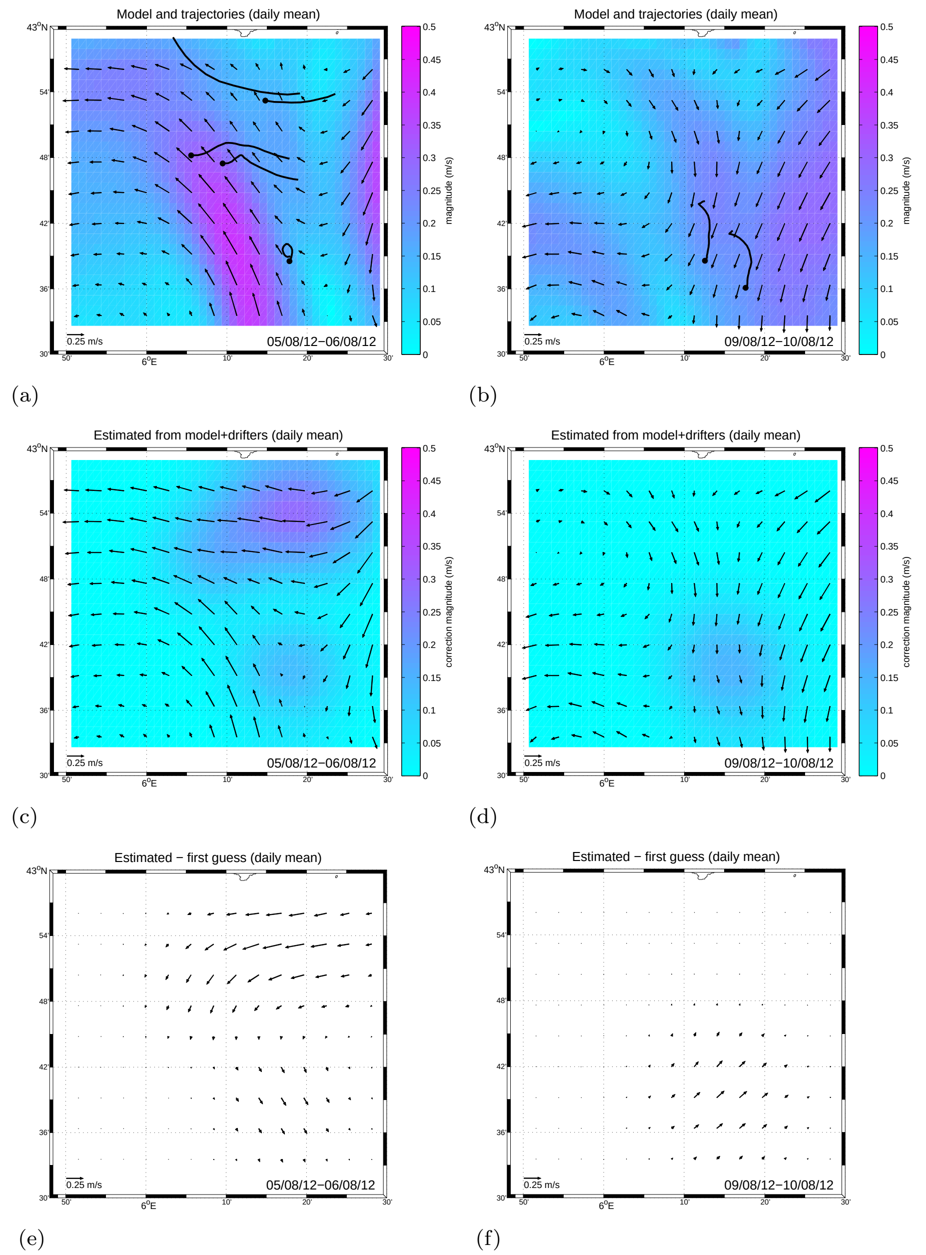

Figure 3: Examples of daily average model velocities for August 5 (left panels) and August 9 (right panels). (a) and (b) show the original velocity fields, with color indicating velocity amplitude and arrows indicating velocity vectors. Drifter trajectories used in LAVA are superimposed; (c),(d) show the LAVA blended fields (E_M), with color indicating the amplitude of the correction C_{daily} (equation 1) and arrows indicating velocity vectors. Panels (e) and (f) represent the vectorial difference between the LAVA estimated and the original velocity field.

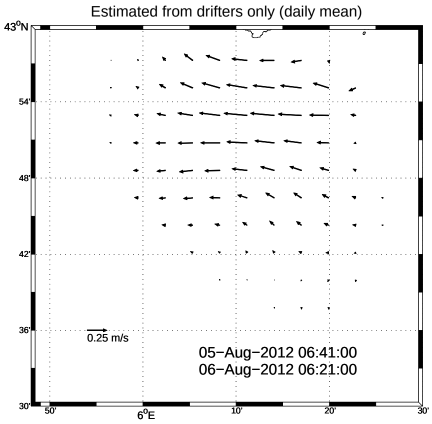

(a)

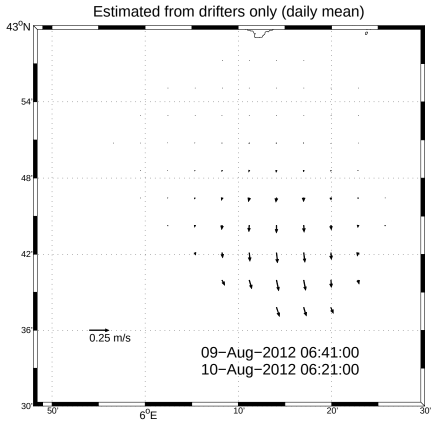

(b)

Figure 4: Examples of daily average velocities reconstructed from drifters only using LAVA (E_D) for August 5 (left panel) and August 9 (right panel). Arrows indicate velocity vectors.

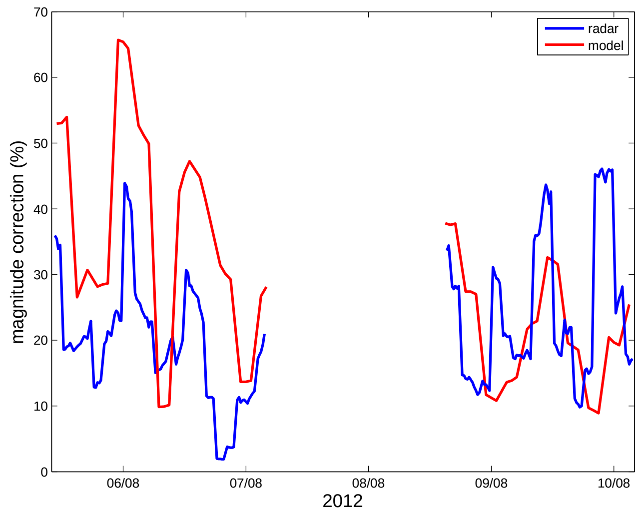

Figure 5: Time series of the normalized correction C_{norm} (equation 2) for radar (blue) and model (red).

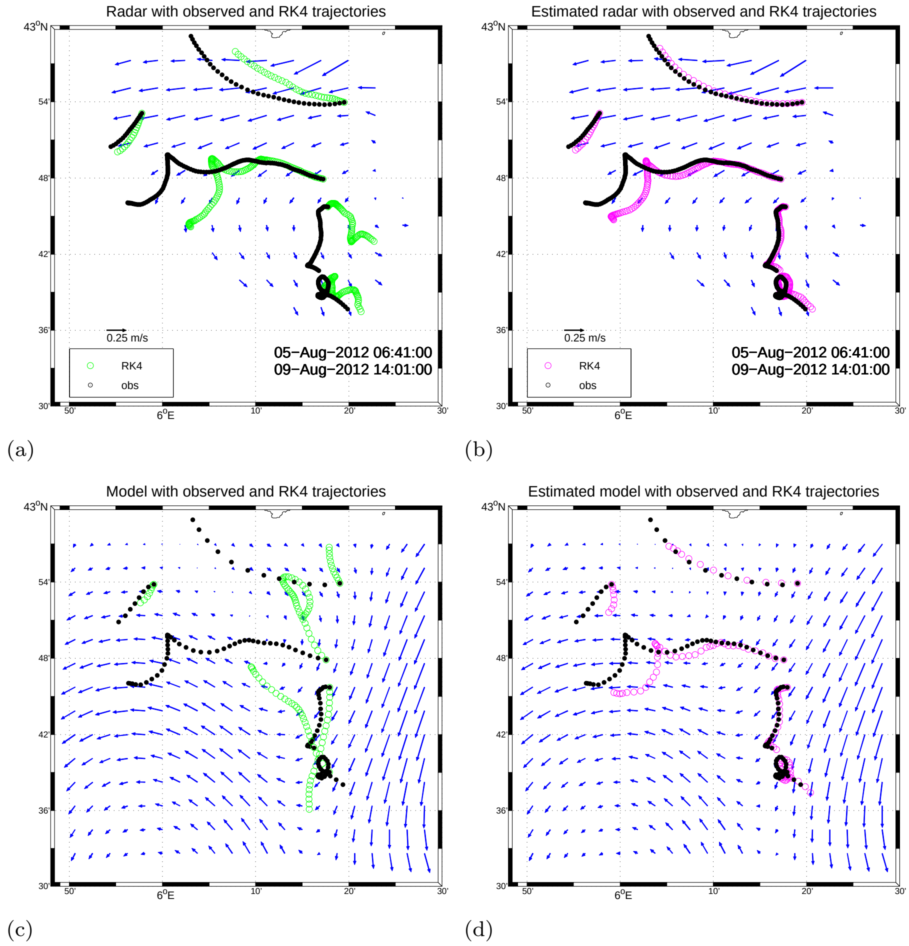

Figure 6: Comparison between observed drifter trajectories (black) and simulated trajectories computed from different velocity fields: (a) original radar velocity; (b) LAVA blended radar velocity; (c) original model velocity; (d) LAVA blended model velocity. The dots corresponds to the positions every Δt (see Table1). The trajectories are superimposed to the corresponding velocity averaged over the period 5-9 August. Arrows size and period considered in the lower panels are as in the upper ones.

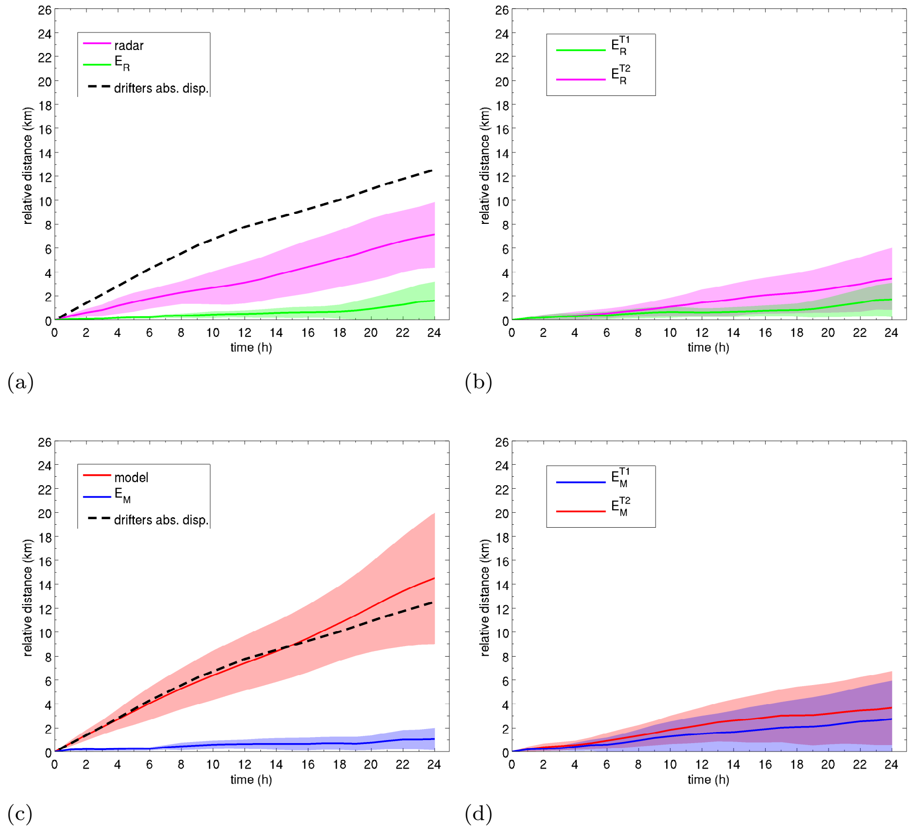

Figure 7: Time series of separation between observed and simulated trajectories $D(t)$ (equation 4) for various cases testing LAVA configurations. $D(t)$ is indicated by color lines (shades indicate standard deviations) and is compared to drifter absolute dispersion $D_0(t)$ (equation 5) indicated by black dashed lines. Upper (lower) panels are for radar (model) velocities. (a) pink line is computed for original radar velocity and green line is for the E_R experiment; (b) green and pink lines are computed for downgraded LAVA E_R^{T1} and E_R^{T2} experiments, respectively. (c) red line is computed for original model velocity and blue line for the E_M experiment; (d) blue and red lines are computed for downgraded LAVA E_M^{T1} and E_M^{T2} experiments, respectively.

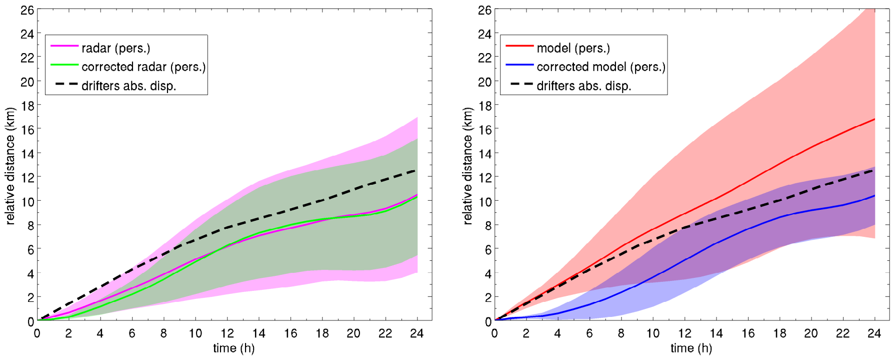

(a) (b)

Figure 8: Time series of separation between observed and simulated trajectories $D(t)$ (equation 4) for various cases testing forecasting skills. The velocity field is held constant in time and trajectories are computed using the frozen field. $D(t)$ is indicated by color lines (shades indicate standard deviations) and is compared to drifter absolute dispersion $D_0(t)$ (equation 5) indicated by black dashed lines. Left (right) panel is for radar (model) velocities. (a) pink line is computed for original radar velocity and green line is for a setup like E_R but with constant radar velocities; (c) red line is computed for original model velocity and blue line is for a setup like E_M but with constant model velocities.

	Experiments						
	E_R	E_M	E_D	E_R^{T1}	E_R^{T2}	E_M^{T1}	E_M^{T2}
first guess velocity	Radar	Model	-	Radar	Radar	Model	Model
N_{Dft}	7	7	7	5	5	5	5
Δx	2 km	1/64°	2 km	2 km	2 km	1/64°	1/64°
Δt	20 min	1 h	20 min	20 min	20 min	1 h	1 h
R	7 km	7 km	7 km	7 km	7 km	7 km	7 km
T_a	2 h	4 h	2 h	2 h	2 h	4 h	4 h
$\overline{d_L}$	247 m	256 m	247 m	1.16 km	3.41 km	1.49 km	3.34 km

Table 1: LAVA parameters used for all experiments (see Section 3.2).

	5-7 aug	8-10 aug
C_{norm} (radar, E_R) (%)	19.21	24.96
C_{norm} (model, E_M) (%)	36.17	21.56
drifters average velocity (m/s)	0.23	0.18

Table 2: Average values of C_{norm} (equation 2) computed during the two periods of drifter coverage (Fig.5) and compared to drifter velocity.